G23A-06

Effects of the Troposphere on GPS and InSAR point target analysis for Measurement of Crustal Deformation and Vertical Motion near Yucca Mountain, Nevada

W.C. Hammond[1], G. Blewitt[1], H.-P. Plag[1], C. Kreemer[1], Z. Li[2]

1) Univeristy of Nevada, Reno, Reno NV, 89557

2) Department of Geographical and Earth Sciences, University of Glasgow, United Kingdom

Introduction

We are in the process of developing a data processing strategy for the systematic integration of InSAR and GPS motion products along the Walker Lane and western Great Basin. This area accommodates ~25% of the relative plate boundary motion between the Pacific and North American Plates, and exhibits complex strain patterns, faulting and seismicity. Thus it is desirable to complement GPS measurements with the high spatial density potentially afforded through InSAR to improve strain maps and block models of crustal deformation.

In preparation for this analysis we have begun a study of the degree of agreement that is possible between deformation signals observed through GPS and InSAR. As a first case study we have selected the Yucca Mountain region of southern Nevada because of 1) availability of numerous ERS and Envisat radar scenes 2) presence of the long running and relatively dense GPS network, 3) usually favorable conditions for GPS and InSAR space geodesy. An important part of this process is the development of metrics that compare the quality of agreement between GPS and InSAR as a function of different data processing strategies.

Currently we are achieving an agreement of ~0.5 mm/yr RMS residual between line of sight rate measurements made using the two separate methods. This is precise enough to possibly improve slip rate estimates in the southern Walker Lane, where slip rates on faults may be an order of magnitude larger than this noise level.

One of the most important contributors to misfit between GPS and InSAR deformation maps is the effects of path delay heterogeneity from the atmosphere. This effect is present in both GPS and InSAR measurements, however, GPS processing software (GIPSY/OASIS in our case) specifically estimates and removes the effects of wet and dry troposphere delays. Thus GPS positions can be provisionally used as a ground truth to which the InSAR-derived line of site maps can be conformed (see figure to right).

Once the scenes covering the Walker Lane are processed, three-component GPS rates and InSAR rates can be simultaneously included as constraints on crustal block models. This requires enhanced block modeling algorithms to model the vertical component of motion. Our formulation (far right) includes vertical and line-of-sight motion, and allows GPS and InSAR constraints can be combined to estimate long term motion of blocks in all three dimensions.

Scenes Available

GeoEarthScope / WinSAR

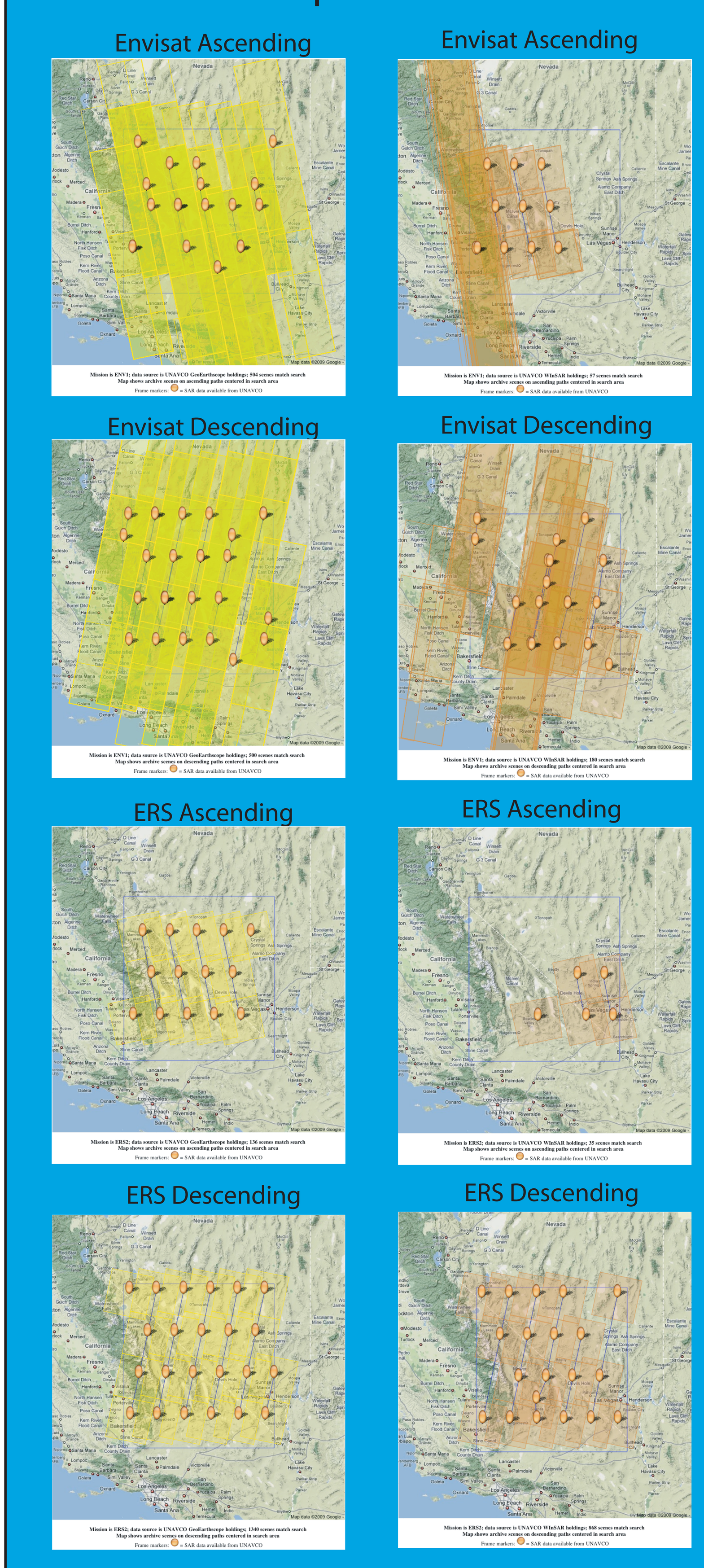

GPS Data and Block Modelling

Below) results of constraining a block model of the southern Walker Lane with horiztonal GPS velocities. See Jha et al., 2009 (oral presentation G23D-07 this meeting) for our most recent results. This modeling will be extended to incorporate line of sight constraints from InSAR, and vertical rates from GPS.

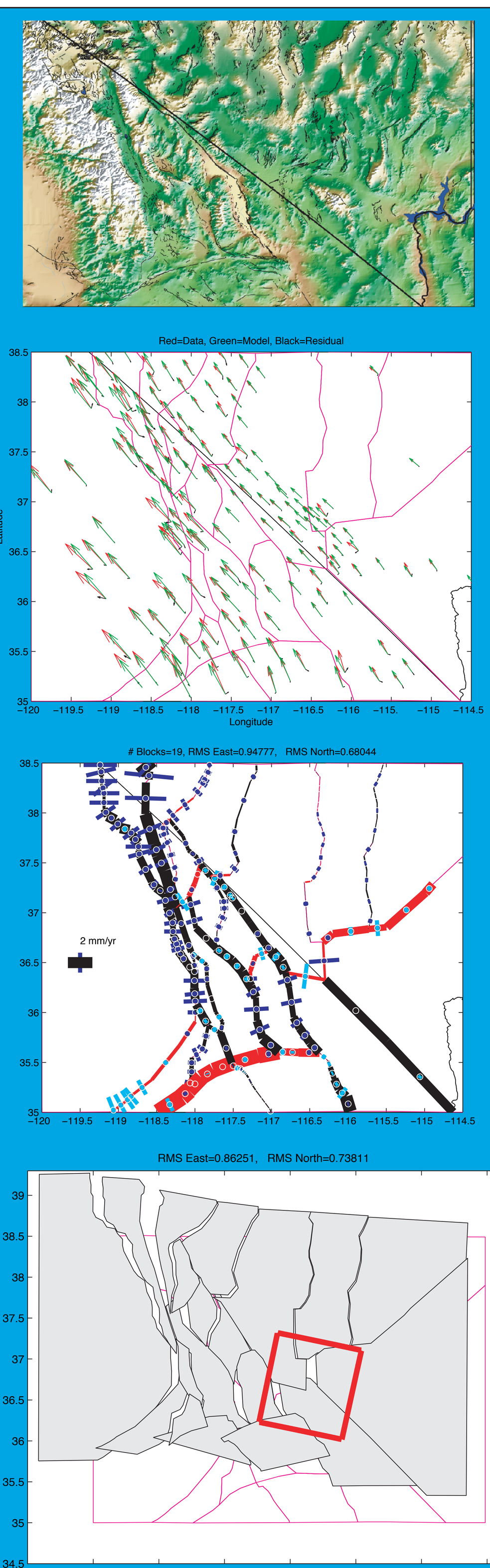

A Beginning - Yucca Mountain...

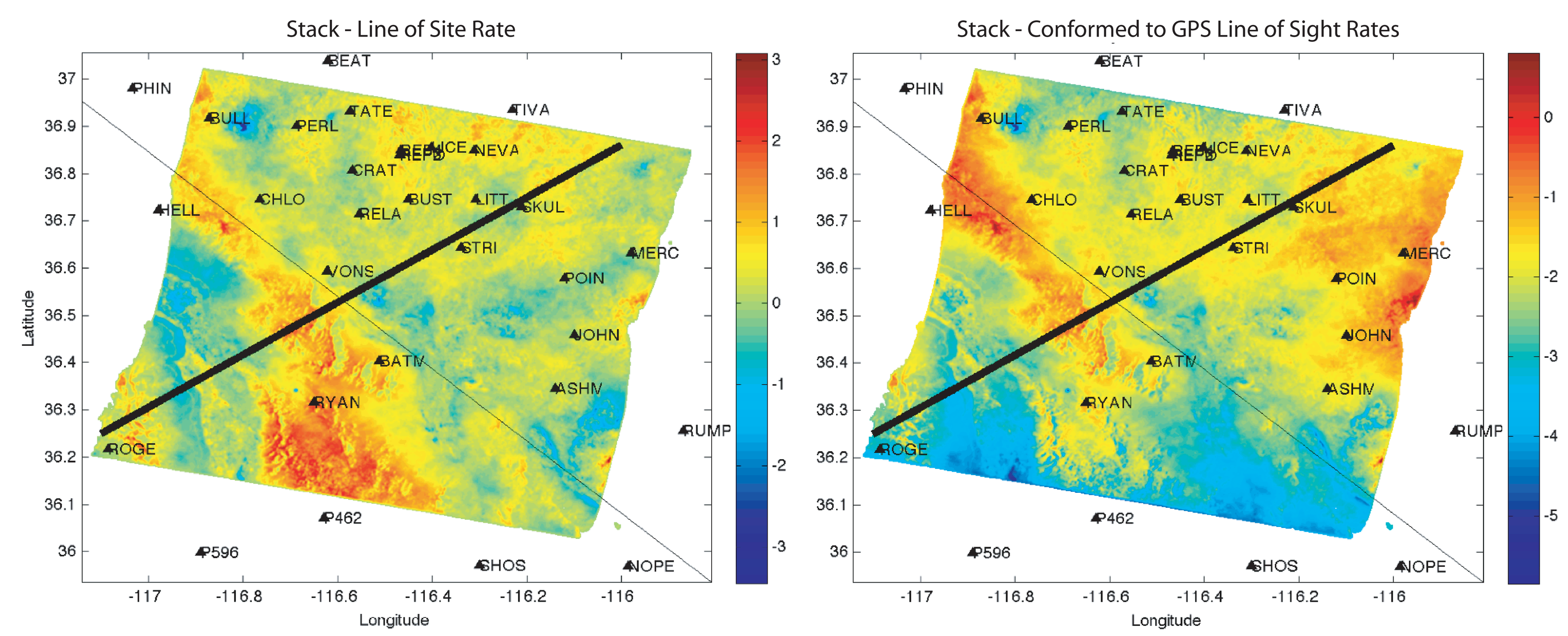

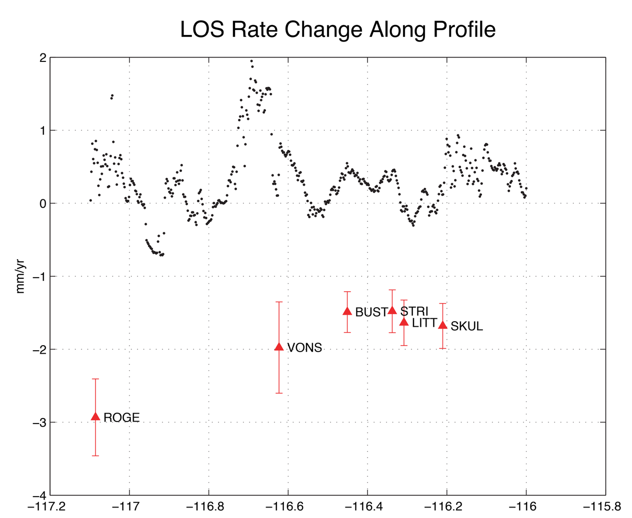

Figures left and right show the rate of motion along the radar line of sight (LOS) from the stack (black dots) and from the LOS component of the nearest GPS sites (red triangles). These are taken along the NE-SW profile shown on the maps above. A best-fitting quadratic ramp is estimated to best conform the radar LOS rates to the GPS velocites. Applying this ramp compensates for long wavelength errors in the interferometry owing to e.g. satellite orbit uncertainty, but does not address shorter wavelength errors (e.g. associated with the atmosphere).

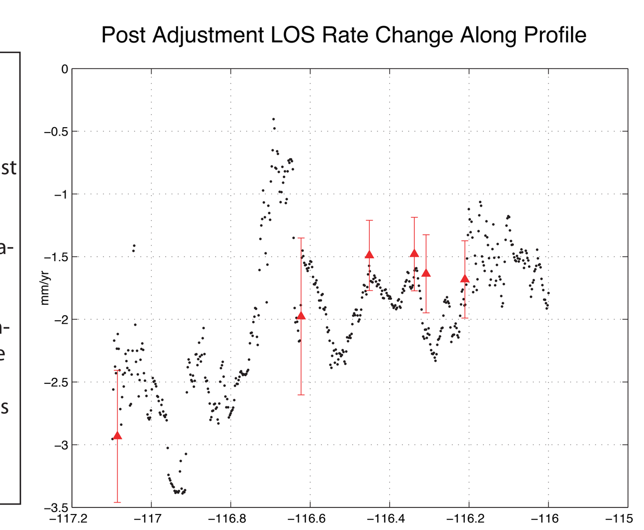

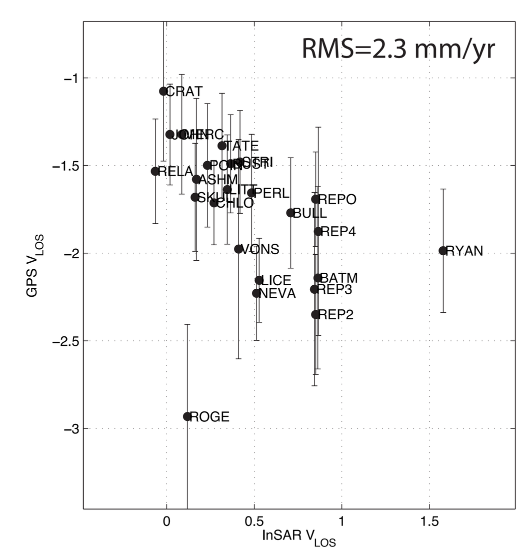

We find that after adjustment the RMS difference between the radar and GPS rates is ~0.5 mm/yr. This measure of similarity between the two rates places limits on how precise crustal deformation estimates using integrated InSAR+GPS motion maps can be. Here we compare the GPS LOS rate to the InSAR LOS rate before adjustment (left) and after adjustment (right). 15 of the 24 sites in the frame have differences that are smaller than the uncertainties in the GPS line of site rates.

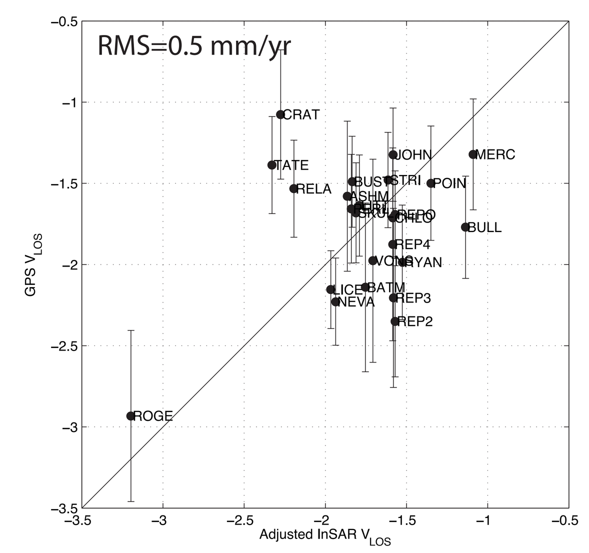

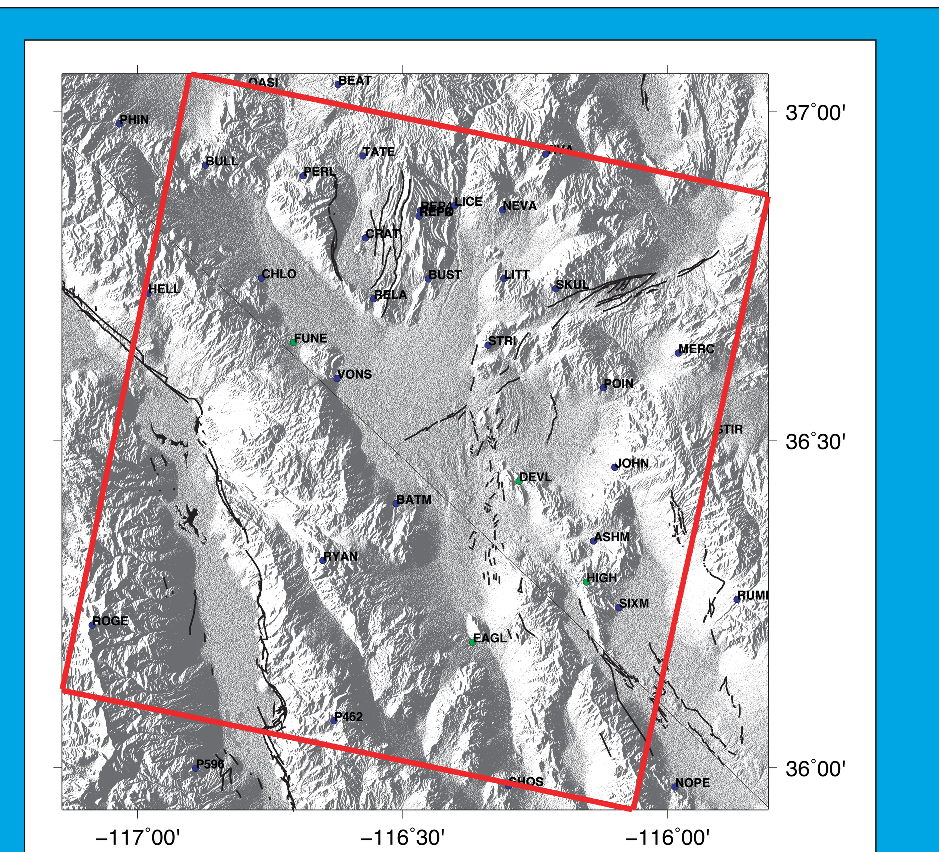

Left) The InSAR data are ERS and Envisat scenes from track 399, frame 2871 (shown in red). For this frame we have 40 ERS and 36 Envisat scenes obtained from the WinSAR and GeoEarthScope archives. Many more scenes are available from nearby tracks in the Walker Lane (far left).

GPS studies have revealed that there is approximately 1 mm/yr of crustal deformation across the Yucca Mountain network of 16 continuous sites [Wernicke et al., 2004; Hill and Blewitt ,2006]. Inside this area are 16 stable GPS sites that have been in operation continuously since late 1999, plus more recently installed stations in the BARGEN and PBO networks.

GPS Atmosphere Estimates

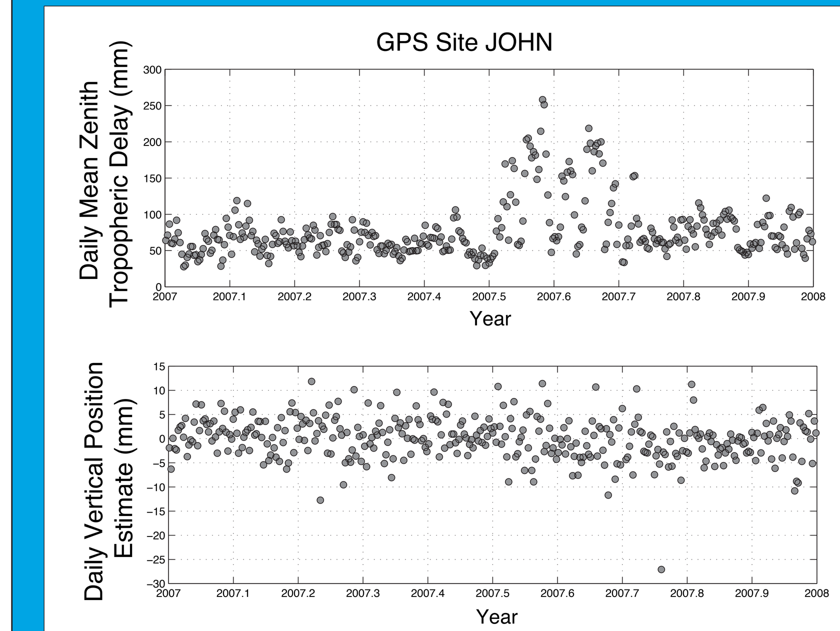

Estimates of GPS satellite to receiver signal delay owing to tropospheric effects are obtained from GIPSY/OASIS II every 5 minutes assuming a random walk model. The magnitude of these effects are 50-250 mm (left and below left), and they can vary by up to 100 mm on any given day (below). Thus these signals are large compared to the expected vertical motions from tectonics.

However, when large changes in the troposphere occur, these singnals are not propagated into the vertical position, suggesting that GIPSY is doing a good job compensating for these effects. Thus GPS can serve as a referece to which InSAR results can be conformed.

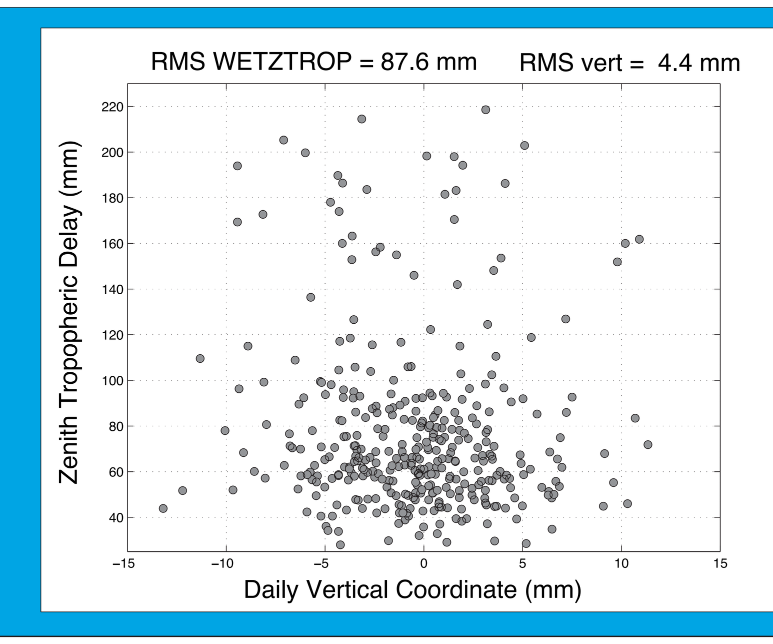

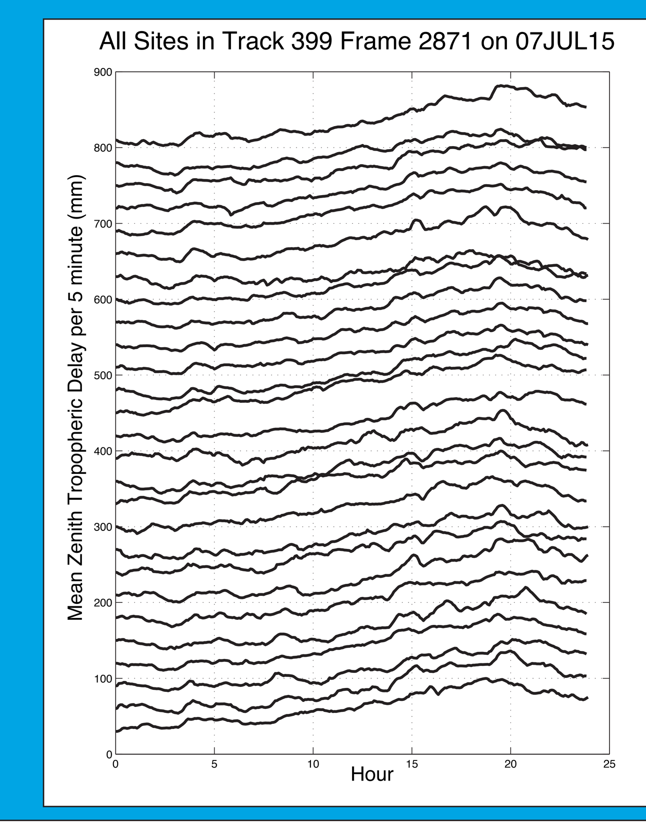

Interferometric Point Scatterers

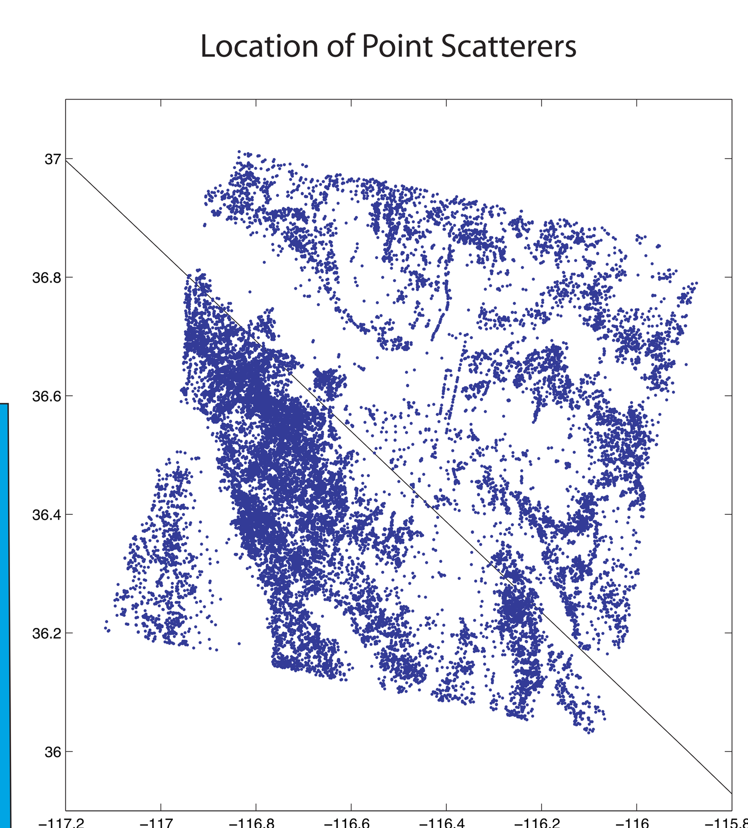

Above) Preliminary identification of point scattering pixels has been made using Gamma IPTA. These points have both the spectral characteristics of a point scatterer and are stable across the ERS and Envisat scenes.

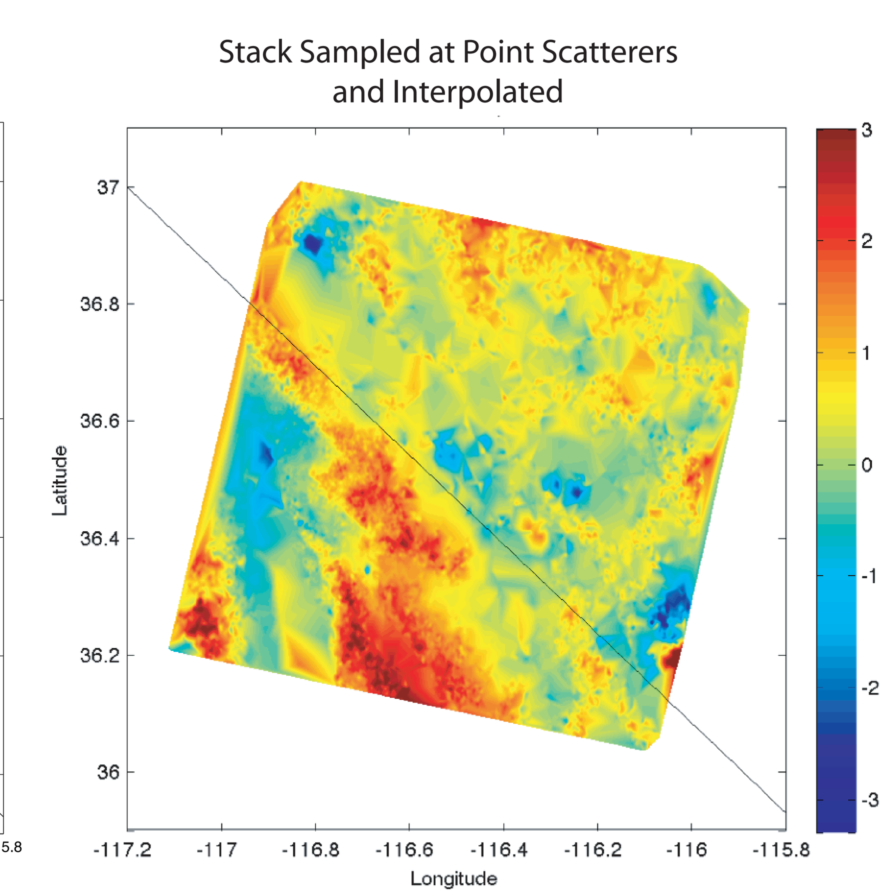

Above) The interferogram stack has been sampled at the point scatterers for comparison to the stack (above left). The same pattern and amplitude of LOS velocity signals persists. We hope that as we improve our analysis the misfit between GPS and InSAR will become even better than 0.5 mm/yr found above.

Block Modelling in the Vertical Dimension and Radar Line of Sight

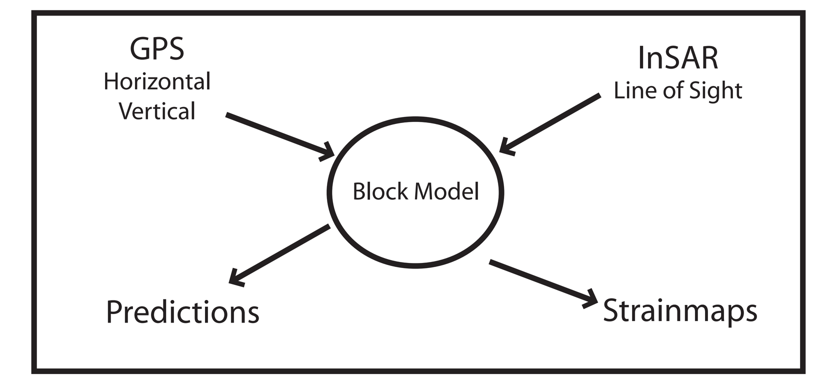

$$\vec{v}_{LT} = \vec{v}_{Int} + \vec{v}_{Cos} \quad (1)$$

$$\vec{v}_{Int} = \vec{v}_{LT} - \vec{v}_{Cos} \quad (2)$$

$$\vec{v}_{GPS,i} = \vec{\omega}_j \times \vec{r}_i + v_{LTU,j}\vec{e}_{U,i} - (a_k\vec{G}_{ss,k} + b_k\vec{G}_{N,k}) \quad (3)$$

$$\vec{v}_{GPS,i} = \vec{\omega}_j \times \vec{r}_i + v_{LTU,j}\vec{e}_{U,i} - \sum_{k=1}^{L}(a_k\vec{G}_{ss,k} + b_k\vec{G}_{N,k}) \quad (4)$$

$$\vec{v}_{N,i} = \left[\vec{\omega}_j \times \vec{r}_i + v_{LTU,j}\vec{e}_{U,i} - \sum_{k=1}^{L}(a_k\vec{G}_{ss,k} + b_k\vec{G}_{N,k})\right] \bullet \vec{e}_{N,i} \quad (5)$$

$$\vec{v}_{E,i} = \left[\vec{\omega}_j \times \vec{r}_i + v_{LTU,j}\vec{e}_{U,i} - \sum_{k=1}^{L}(a_k\vec{G}_{ss,k} + b_k\vec{G}_{N,k})\right] \bullet \vec{e}_{E,i} \quad (6)$$

$$\vec{v}_{U,i} = \left[v_{LTU,j}\vec{e}_{U,i} - \sum_{k=1}^{L}(a_k\vec{G}_{ss,k} + b_k\vec{G}_{N,k})\right] \bullet \vec{e}_{U,i} \quad (7)$$

$$\vec{v}_{los,i} = \left[\vec{\omega}_j \times \vec{r}_i + v_{LTU,j}\vec{e}_{U,i} - \sum_{k=1}^{L}(a_k\vec{G}_{ss,k} + b_k\vec{G}_{N,k})\right] \bullet \vec{e}_{los,i} \quad (8)$$

$$\vec{v}_{N,i} = \left[\vec{\omega}_j \times \vec{r}_i - \sum_{k=1}^{L}(a_k\vec{G}_{ss,k} + b_k\vec{G}_{N,k})\right] \bullet \vec{e}_{N,i} - \varepsilon_{\phi\theta} r_0 \sin\theta_0 \Delta\phi - \varepsilon_{\theta\theta} r_0 \Delta\theta \quad (9)$$

$$\vec{v}_{E,i} = \left[\vec{\omega}_j \times \vec{r}_i - \sum_{k=1}^{L}(a_k\vec{G}_{ss,k} + b_k\vec{G}_{N,k})\right] \bullet \vec{e}_{E,i} + \varepsilon_{\phi\phi} r_0 \sin\theta_0 \Delta\phi + \varepsilon_{\phi\theta} r_0 \Delta\theta \quad (10)$$

$$\vec{v}_{los,i} = \left[\vec{\omega}_j \times \vec{r}_i - \sum_{k=1}^{L}(a_k\vec{G}_{ss,k} + b_k\vec{G}_{N,k})\right] \bullet \vec{e}_{los,i} + \left(T_{neu\rightarrow xyz}\begin{bmatrix} -\varepsilon_{\phi\theta} r_0 \sin\theta_0 \Delta\phi - \varepsilon_{\theta\theta} r_0 \Delta\theta \\ \varepsilon_{\phi\phi} r_0 \sin\theta_0 \Delta\phi + \varepsilon_{\phi\theta} r_0 \Delta\theta \\ 0 \end{bmatrix}\right) \bullet \vec{e}_{los,i} \quad (11)$$

$$\vec{\omega}_{j_1} \times \vec{p}_k - \vec{\omega}_{j_2} \times \vec{p}_k + \left(v_{LTU,j_1} - v_{LTU,j_2}\right)\vec{e}_{U,i} = a_k\delta\vec{G}_{SS,k} + b_k\delta\vec{G}_{N,k} \quad (12)$$

$$\delta\vec{G}_{SS,k} = \vec{G}_{SS}(\vec{p}_k + \vec{\varepsilon}) - \vec{G}_{SS}(\vec{p}_k - \vec{\varepsilon}) \quad (13)$$

$$\delta\vec{G}_{N,k} = \vec{G}_{N}(\vec{p}_k + \vec{\varepsilon}) - \vec{G}_{N}(\vec{p}_k - \vec{\varepsilon}) \quad (14)$$

$$\vec{u} \bullet (\vec{v} \times \vec{w}) = -\vec{v} \bullet (\vec{u} \times \vec{w}) \quad (15)$$

$$v_{N,i} = -\vec{\omega}_j \bullet (\vec{e}_{N,i} \times \vec{r}_i) - \left[\sum_{k=1}^{L}(a_k\vec{G}_{ss,k} + b_k\vec{G}_{N,k})\right] \bullet \vec{e}_{N,i} - \varepsilon_{\phi\theta} r_0 \sin\theta_0 \Delta\phi - \varepsilon_{\theta\theta} r_0 \Delta\theta \quad (16)$$

$$v_{E,i} = -\vec{\omega}_j \bullet (\vec{e}_{E,i} \times \vec{r}_i) - \left[\sum_{k=1}^{L}(a_k\vec{G}_{ss,k} + b_k\vec{G}_{N,k})\right] \bullet \vec{e}_{E,i} + \varepsilon_{\phi\phi} r_0 \sin\theta_0 \Delta\phi + \varepsilon_{\phi\theta} r_0 \Delta\theta \quad (17)$$

$$v_{U,i} = v_{LTU,i} - \left[\sum_{k=1}^{L}(a_k\vec{G}_{ss,k} + b_k\vec{G}_{N,k})\right] \bullet \vec{e}_{U,i} \quad (18)$$

$$\begin{aligned} \vec{v}_{los,i} = &-\vec{\omega}_j \bullet \left(\vec{e}_{los,i} \times \vec{r}_i\right) - \left[\sum_{k=1}^{L}(a_k\vec{G}_{ss,k} + b_k\vec{G}_{N,k})\right] \bullet \vec{e}_{los,i} + \\ &\varepsilon_{\phi\theta} r_0\left[-\sin\theta_0\Delta\phi\left(T_{i,1}^{-1} \bullet \vec{e}_{los,i}\right) + \Delta\theta\left(T_{i,2}^{-1} \bullet \vec{e}_{los,i}\right)\right] + , \\ &\varepsilon_{\theta\theta} r_0 \Delta\theta\left(-T_{i,1}^{-1} \bullet \vec{e}_{los,i}\right) + \\ &\varepsilon_{\phi\phi} r_0 \sin\theta_0 \Delta\phi\left(T_{i,2}^{-1} \bullet \vec{e}_{los,i}\right) \end{aligned} \quad (19)$$

$$\begin{aligned} &\vec{\omega}_{j_1} \bullet (-\vec{e}_{N,k} \times \vec{p}_k) + \vec{\omega}_{j_2} \bullet (\vec{e}_{N,k} \times \vec{p}_k) - \varepsilon_{\phi\theta 1} r_0 \sin\theta_{k0}\Delta\phi_1 - \varepsilon_{\theta\theta 1} r_0 \Delta\theta_1 + \varepsilon_{\phi\theta 2} r_0 \sin\theta_{k0}\Delta\phi_2 + \varepsilon_{\theta\theta 2} r_0 \Delta\theta_2 \\ &= \left(a_k\delta\vec{G}_{SS,k} + b_k\vec{G}_{N,k}\right) \bullet \vec{e}_N \end{aligned} \quad (20)$$

$$\begin{aligned} &\vec{\omega}_{j_1} \bullet (-\vec{e}_{E,k} \times \vec{p}_k) + \vec{\omega}_{j_2} \bullet (\vec{e}_{E,k} \times \vec{p}_k) - \varepsilon_{\phi\phi 1} r_0 \sin\theta_{k0}\Delta\phi_1 - \varepsilon_{\phi\theta 1} r_0 \Delta\theta_1 + \varepsilon_{\phi\phi 2} r_0 \sin\theta_{k0}\Delta\phi_2 + \varepsilon_{\phi\theta 2} r_0 \Delta\theta_2 \\ &= \left(a_k\delta\vec{G}_{SS,k} + b_k\vec{G}_{N,k}\right) \bullet \vec{e}_E \end{aligned} \quad (21)$$

$$v_{LTU,j_1} - v_{LTU,j_2} = \left(a_k\delta\vec{G}_{SS,k} + b_k\vec{G}_{N,k}\right) \bullet \vec{e}_{U,k} = b_k \sin(\delta) \quad (22)$$

Acknoweldgements

This work is supported by the NASA ROSES EarthScope Geodetic Imaging Program (project NNX09AD24G), and the NSF EarthScope Program (projet 0844389). We use the GAMMA software for processing of radar data. GPS data were obtained from the UNAVCO, Inc. data archive. InSAR data were obtained from the WinSAR and GeoEarthScope archives via UNAVCO, Inc.

References

Hill, E., and G. Blewitt (2006), Testing for fault activity at Yucca Mountain, Nevada, using independent GPS results from the BARGEN network, Geophysical Research Letters, 33, L14302, doi:10.1029/2006GL026140.

Jha, S., W.C. Hammond, C. Kreemer, G. Blewitt, New GPS constraints on Owens Valley fault slip rates, Eos Trans. AGU, 90(54) Fall Meet. Suppl., Abstract G23D-07, December 14-18, 2009.

Wernicke, B. P., J. L. Davis, R. A. Bennett, J. E. Normandeau, A. M. Friedrich, and N. A. Niemi (2004), Tectonic Implications of a dense continuous GPS velocity field at Yucca Mountain, Nevada, Journal of Geophysical Research, 109, B12404.